

Fluid Forces or Impacts, What Governs the Entrainment of Soil Particles in Sediment Transport Mediated by a Newtonian fluid?

Thomas Pähtz^{1,2*} and Orencio Durán³

1. *Institute of Port, Coastal and Offshore Engineering,
Ocean College, Zhejiang University, 310058 Hangzhou, China*

2. *State Key Laboratory of Satellite Ocean Environment Dynamics,
Second Institute of Oceanography, 310012 Hangzhou, China*

3. *Department of Physical Sciences, Virginia Institute of Marine Sciences,
College of William and Mary, 23062 Williamsburg, USA*

In steady sediment transport, sediment deposition is balanced by entrainment through fluid forces or particle-bed impacts. Here we show that transport is fully impact-sustained when $\text{Im} = \text{Re}_p \sqrt{s} + 0.5 \gtrsim 20$ or $\Theta \gtrsim 5/\text{Im}$, where s is the particle-fluid-density ratio, Re_p a particle Reynolds number, and Θ the dimensionless fluid shear stress. Fully impact-sustained transport causes a linear scaling of the transport rate with Θ . However, for bedload, this scaling becomes non-linear slightly above the threshold, which we propose is linked to the formation of a liquid-like bed on top of the static-bed surface.

PACS numbers: 45.70.-n, 47.55.Kf, 92.40.Gc

Sediment transport in a Newtonian fluid, such as water and air, is one of the most important geological processes responsible for the alteration of sea and river-scapes, and dry planetary surfaces [1–12]. It can occur in a large variety of natural environments, e.g., viscous and turbulent transport of minerals and organics by Earth’s water streams [1–5], turbulent transport of dust and sand by Earth’s atmospheric winds [7–11], and wind-driven transport of minerals on planetary bodies with extremely thin atmospheres, such as Triton, Pluto, and comet 67P/Churyumov-Gerasimenko [12].

Different sediment transport regimes are documented. Very small particles, whose weight can be fully supported by the fluid turbulence, tend to be transported in turbulent suspensions [5, 10]. Medium and large particles, on the other hand, are transported close to the surface, in trajectories not much influenced by fluid turbulence [5, 10]. The latter case includes bedload and saltation. Bedload refers to particles rolling, sliding, and hopping in the vicinity of the sediment bed, which is typical for the transport of sand and gravel by water streams [13, 14]. Saltation refers to particles moving in ballistic trajectories along the bed, which is typical for the transport of sand by planetary winds [9–11].

It has become a widely-accepted hypothesis that the mechanisms sustaining bedload and saltation are fundamentally different: bedload being sustained through entrainment of soil bed particles directly by fluid forces [14–35] and saltation being sustained through particle-bed impacts ejecting bed particles [36–42], allowing transport even below the fluid entrainment threshold [9–12, 43–47]. However, recent studies questioned this hypothesis by suggesting that transport below the fluid entrainment threshold is also possible for turbulent bedload [48], and by showing that an analytical model taking into account particle dynamics is able to reproduce measurements of

bedload and saltation thresholds at the same time [12].

Here we carry out direct numerical simulations of sediment transport in a Newtonian fluid with a model that couples a discrete element method for the particle motion and a continuum Reynolds-averaged description of hydrodynamics (for details, see Ref. [49]), which belongs to a new generation of sophisticated grain-scale models of sediment transport [12, 48–60]. Visual inspection of the simulations show that particle-bed impacts are, indeed, predominantly responsible for the entrainment of bed sediment in turbulent bedload. Furthermore, we find that the characteristic horizontal velocity of particles moving near the the bed surface, hereafter called ‘bed velocity’ V_b , in units of \sqrt{gd} becomes approximately constant when a critical ‘impact number’ $\text{Im} = \text{Re}_p \sqrt{s} + 0.5 \approx 20$ is exceeded, where $s = \rho_p/\rho_f$ is the particle-fluid-density ratio and $\text{Re}_p = \sqrt{(s-1)gd^3}/\nu$ the particle Reynolds number, with $g [\hat{g} = (s-1)g/(s+0.5)]$ the gravitational constant [reduced by buoyancy and added mass], d the mean particle diameter, and ν the kinematic viscosity. Though not strictly proven, a constant average horizontal particle velocity near the bed surface is widely recognized as a signature of sediment transport that is fully sustained through sediment entrainment caused by particle-bed impacts [9, 44–47, 61–65] and has been confirmed in aeolian wind tunnel and field measurements [66–71]. The fact that the condition $\text{Im} \gtrsim 20$ includes the turbulent bedload regime is thus strong evidence that also turbulent bedload is fully sustained through particle-bed impact entrainment. We would like to emphasize that all results presented in this letter for the bedload regime usually do not significantly depend on contact parameters, such as the restitution coefficient e and contact friction coefficient μ^c . For instance, bedload simulations with $e = 0.9$ and $e = 0.01$ are nearly exactly the same on average, which is consistent

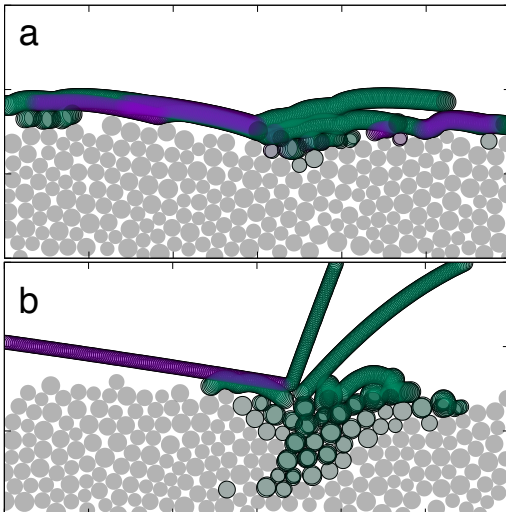


FIG. 1. Visualizations of impact entrainment events for (a) turbulent bedload ($s = 2.65$, $Re_p = 20$, $\sqrt{\Theta} = 0.33$) and (b) saltation ($s = 2000$, $Re_p = 20$, $\sqrt{\Theta} = 0.08$) from direct transport simulations near the threshold. The purple and green colors indicate the trajectory of particles before and after impact, respectively. Particles move from the left to the right.

with previous reports [59]. This finding implies that any dissipative interaction force that is proportional to the relative velocity of two approaching particles and acts at and/or close to particle contact, such as the lubrication force [72], does not significantly influence average bedload transport characteristics because the effect of such forces can be incorporated in e and μ_c [56, 59, 73, 74].

Results.—We carried out simulations for s and Re_p within the range $s \in [2.65, 2000]$ and $Re_p \in [0.1, 100]$ and for $s = 10^7$ and $Re_p = 0.1$. For each pair of s and Re_p , we varied the dimensionless fluid shear stress (“Shields parameter”) $\Theta = \tau / [(\rho_p - \rho_f)gd]$ in regular intervals and obtained the cessation threshold (Θ_t^{ex}) through extrapolation to vanishing sediment transport [49].

Figure 1 shows snapshots of transport simulations near Θ_t^{ex} for turbulent bedload (Fig. 1a) and saltation (Fig. 1b) shortly before and after an impact entrainment event (see also Movies S1 and S2). In both cases, a transported particle collides with one or more bed particles, which subsequently become mobilized with a short time delay. In bedload, the transported particle impacts the bed from a very small height and entrains a bed particle by dragging it out of its trap, while in saltation, the transported particle impacts the bed from a very large height and entrains a bed particle by ejecting it. Close to the threshold, impact entrainment events are rare in both cases as impacts occur much less often, but are much more effective in saltation than they are in turbulent bedload (Movies S1 and S2). As a consequence,

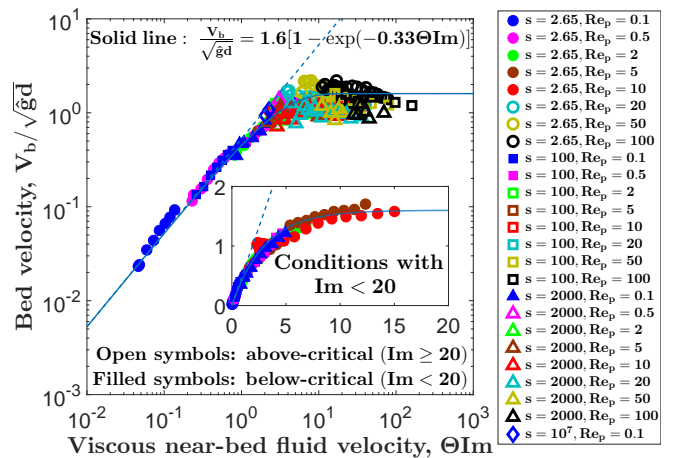


FIG. 2. Dimensionless bed velocity V_b/\sqrt{gd} versus dimensionless, viscous, horizontal near-bed fluid velocity ΘIm for various s , Re_p , and Θ in log-log scale. Inset: Same in linear-linear scale for cases with $\text{Im} < 20$.

bed particles remain in repose most of the time because fluid forces are too weak to entrain them directly. Sufficiently far from the threshold, impact entrainment events occur much more often in saltation (Movie S3), whereas it is impossible to determine single entrainment events in turbulent bedload as several layers of the bed are in continuous motion (Movie S4).

The relevance of impact entrainment relative to direct fluid entrainment for arbitrary conditions can be indirectly quantified by the relation between the dimensionless bed velocity V_b/\sqrt{gd} and the dimensionless, viscous, horizontal near-bed fluid velocity $U_b^{\text{vis}}/\sqrt{gd} \propto u_*^2 d / (\nu\sqrt{gd}) \equiv \Theta\text{Im}$ (Fig. 2). In our transport simulations, we obtain V_b from averaging the vertical profile of the horizontal particle velocity gradient near the bed surface. For saltation transport, our definition yields values of V_b about equal to the classical ‘slip velocity’ (i.e., the average particle velocity at the bed surface [70]), but in contrast to the latter, our definition makes also sense for bedload transport conditions (Suppl. Mat. [75]). When sediment transport is fully sustained through fluid entrainment, the bed velocity scales with the average near-bed fluid velocity (dashed line in Fig. 2). In contrast, when sediment transport is fully sustained through impact entrainment, the dimensionless bed velocity is approximately constant, $V_b/\sqrt{gd} \approx 1.6$, and barely changes with Θ , s , and Re_p (part of the variation can be attributed to small changes the bed friction coefficient, see Fig. S2 in the Suppl. Mat. [75]). A constant bed velocity ensures that, on average, exactly one particle leaves the bed per impacting particle [9, 44–47, 61–65].

The transition to a fully impact-sustained transport regime is determined by two independent conditions. First, the impact number $\text{Im} = Re_p\sqrt{s} + 0.5$ has to

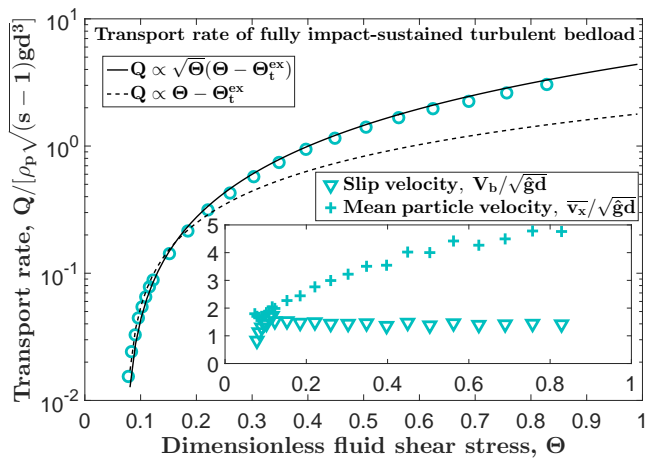


FIG. 3. Dimensionless sediment transport rate $Q/[\rho_p \sqrt{(s-1)gd^3}]$ versus dimensionless fluid shear stress Θ for fully impact-sustained bedload transport ($s = 2.65$ and $Re_p = 20$). Inset: Dimensionless transport-layer-averaged horizontal particle velocity $\bar{v}_x/\sqrt{\hat{g}d}$ and bed velocity $V_b/\sqrt{\hat{g}d}$ versus Θ .

exceed a critical value: $Im \gtrsim 20$ (Fig. 2, open symbols). This follows from the fact that the transport-layer average \bar{v}_x of the horizontal particle velocity v_x (defined in Suppl. Mat. [75]) must be larger than the bed velocity since v_x increases with height. For relatively viscous conditions at grain scale ($Re_p < 5$) and close to the transport threshold (Θ_t^{ex}), the scaling of the average particle velocity \bar{v}_x can be obtained from the proportionality of \bar{v}_x with the transport-layer average fluid velocity \bar{u}_x (Fig. 4) and a dynamic-friction condition (i.e., $\bar{u}_x - \bar{v}_x \propto Re_p \sqrt{(s-1)gd}$ [45]). Thus, $\bar{v}_x \propto Re_p \sqrt{(s-1)gd} = Im \sqrt{\hat{g}d}$ and the condition $\bar{v}_x > V_b \approx \sqrt{\hat{g}d}$ implies $Im > Im_c$, with $Im_c \approx 20$.

The second condition for fully impact-sustained transport is $\Theta \gtrsim 5/Im$ and follows from the proportionality of the dimensionless bed velocity with the dimensionless, viscous, horizontal near-bed fluid velocity in the fully fluid-sustained regime ($V_b/\sqrt{\hat{g}d} \propto \Theta Im$) and the fact that $V_b/\sqrt{\hat{g}d}$ cannot increase indefinitely (Fig. 2). Therefore, for $Im < 20$, which exclusively characterizes viscous bedload conditions, increasing the Shields parameter leads to a transition from fully fluid-sustained when $\Theta \lesssim 1/Im$ to fully impact-sustained transport when $\Theta \gtrsim 5/Im$ as the increasing bed velocity reaches the maximum value needed to replace every particle trapped at the bed by exactly one entrained particle (inset of Fig. 2). Note that, near the threshold, the condition $\Theta \gtrsim 5/Im$ always implies $Im \gtrsim 20$ (i.e., $\Theta_t^{\text{ex}} < 0.25$ [76]), but not vice versa (e.g., $s = 10^7$, $Re_p = 0.1$ in Fig. 2).

Implications.—It is commonly assumed that a constant dimensionless slip and thus bed velocity in the fully impact-sustained regime implies that the average hori-

zontal particle velocity \bar{v}_x is also constant [38, 46, 47] or nearly constant [43–45, 61, 77], and that the sediment transport rate therefore approximately scales as $Q \propto \Theta - \Theta_t^{\text{ex}}$. However, we find this assumption is not valid for fully impact-sustained bedload transport (Fig. 3). Although Q is, indeed, linear in Θ when $\Theta \lesssim 2\Theta_t^{\text{ex}}$, it transforms into a $\Theta^{1.5}$ -dependency when $\Theta \gtrsim 2\Theta_t^{\text{ex}}$. As a consequence, the scaling $Q \propto \sqrt{\Theta}(\Theta - \Theta_t^{\text{ex}})$, which is consistent with measurements of the bedload transport rate [78–80], provides a much better overall fit to the simulations.

The transition from a linear to a non-linear transport law for turbulent bedload is consistent with a transition from a constant average particle velocity (\bar{v}_x) to one that increases with Θ , which occurs even though the bed velocity V_b remains nearly constant (inset of Fig. 3). A similar transition in $\bar{v}_x(\Theta)$ can be found for some other fully impact-sustained conditions (inset of Fig. 5 and Fig. S3) and a similar lack of correlation of \bar{v}_x with V_b , and also with the classical slip velocity, for all fully impact-sustained conditions (Fig. S3).

As shown in Fig. 4, the horizontal particle velocity scales with the horizontal fluid velocity and not with the bed velocity, which just represents a lower bound for \bar{v}_x . The scaling of \bar{v}_x with the transport-layer-averaged fluid velocity \bar{u}_x follows from the relation between \bar{v}_x and the size of the transport layer (\bar{z}). When the transport layer is within the viscous sublayer of the turbulent boundary layer ($\bar{z}/z_\nu \lesssim 5$, with the viscous length $z_\nu \equiv d/[\sqrt{\Theta}Re_p]$), \bar{v}_x scales with the characteristic fluid velocity within the viscous sublayer: $\bar{v}_x \propto \bar{u}_x$, where \bar{u}_x scales as $\bar{u}_x \approx \sqrt{\Theta(s-1)gd} \bar{z}/z_\nu$ when the particle-flow feedback (see below) can be neglected. On the other hand, when the transport layer extends beyond the viscous sublayer, the scale of the particle velocity is dominated by the characteristic fluid velocity in the logarithmic region of the velocity profile. That is, $\bar{v}_x \propto \sqrt{\Theta(s-1)gd} \equiv u_*$ when the particle-flow feedback can be neglected.

However, for turbulent saltation transport ($s = 2000$, $Re_p \gtrsim 5$), there is a strong negative feedback on the flow generated by particle motion [81–83], which is a necessary condition to maintain a constant slip and thus bed velocity [9]. As a consequence, the fluid shear velocity remains approximately constant with Θ in an extended region above the bed surface, and the particle velocity scales as $\bar{v}_x \propto \sqrt{\Theta_t^{\text{ex}}(s-1)gd} \equiv u_t^{\text{ex}}$ (inset of Fig. 4), resulting in a linear scaling of Q with Θ , consistent with measurements [70, 71, 84]. We propose that the same negative feedback keeps a constant average particle velocity, at least close enough to the threshold, in all fully impact-sustained regimes (inset of Fig. 4), including turbulent bedload. However, the simulations suggest that, at sufficiently large fluid shear stresses ($\Theta \gtrsim 2\Theta_t^{\text{ex}}$ for turbulent bedload), a highly collisional layer of transported particles (a liquid-like or ‘soft’ bed [51]) develops because

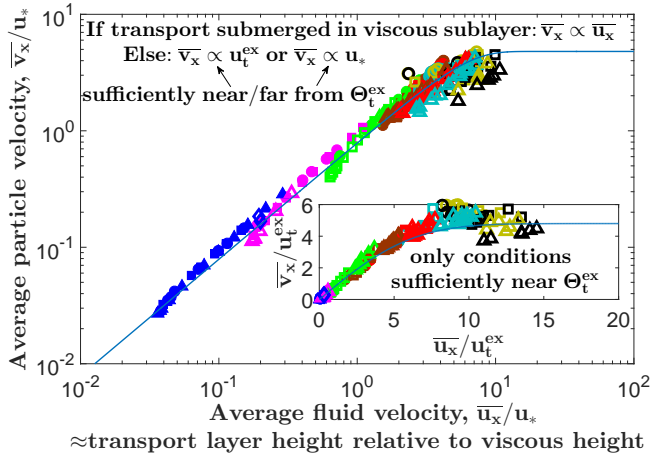


FIG. 4. Average particle velocity \bar{v}_x versus average fluid velocity \bar{u}_x , both rescaled by the fluid shear velocity u_* , for various s , Re_p , and Θ . Inset: The same in linear-linear scale, but both velocities rescaled by the fluid shear velocity at the threshold (u_t^{ex}). Among the fully impact-sustained simulation cases, only those corresponding to the linear transport rate regime are shown in the inset (see text). The solid lines correspond to $\bar{v}_x/u_*^{\text{typ}} = 4.8\sqrt{1 - \exp[-0.027(\bar{u}_x/u_*^{\text{typ}})^2]}$, where $u_*^{\text{typ}} = u_*$ (main figure) or $u_*^{\text{typ}} = u_t^{\text{ex}}$ (inset). For symbol legend, see Fig. 2.

the bed surface becomes completely mobile (‘stage-3 bedload’ [14]). This liquid-like bed hinders particles moving over it from reaching the disturbed-flow region near the quasi-static-bed surface as they tend to rebound from the liquid-bed surface (Movie S4). Hence, these particles can remain extended periods of time in the nearly-undisturbed-flow region, leading to an increase of \bar{v}_x with Θ . This point is further supported by Fig. 5, which shows that, for fully impact-sustained conditions with increasing \bar{v}_x , the beginning increase of \bar{v}_x (inset of Fig. 5) approximately coincides with a beginning increase of the effective location of energetic particle rebounds relative to the quasi-static bed.

Conclusion.—Our study challenges the paradigm that sediment transport mediated by water [14, 22, 33] or heavy air [10, 47, 85], like on Venus and Titan, is sustained through direct fluid entrainment of bed particles. In fact, we have shown that the average horizontal near-bed particle velocity (‘bed velocity’) in natural units (V_b/\sqrt{gd}) becomes a universal constant when the ‘impact number’ $\text{Im} = \text{Re}_p\sqrt{s} + 0.5 \gtrsim 20$ or $\Theta \gtrsim 5/\text{Im}$, indicating that sediment transport is sustained solely through particle-bed impacts. $\text{Im} \gtrsim 20$ includes nearly all relevant sediment transport regimes. Only sufficiently viscous bedload transport is sustained, at least partially, through direct fluid entrainment ($\text{Im} \lesssim 20$).

Our study further challenges the very common assumption in saltation transport modeling that the entire par-

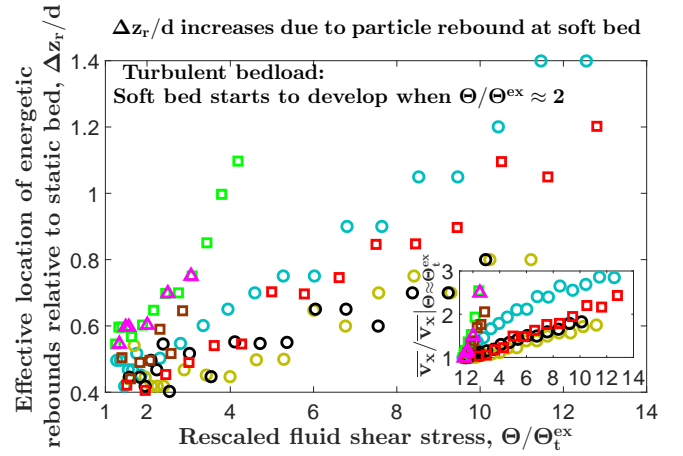


FIG. 5. Effective location of energetic rebounds relative to the quasi-static bed (Δz_r), defined through a maximum of the rate of fluctuation energy production (Suppl. Mat. [75]), versus rescaled dimensionless fluid shear stress ($\Theta/\Theta_t^{\text{ex}}$) for fully impact-sustained conditions with increasing \bar{v}_x . Inset: Rescaled average particle velocity $\bar{v}_x/\bar{v}_x|_{\Theta \approx \Theta_t^{\text{ex}}}$ versus $\Theta/\Theta_t^{\text{ex}}$. For symbol legend, see Fig. 2.

ticle motion can be represented by particles moving in identical trajectories [7, 9, 38, 46, 47, 63, 86–93]. If this assumption was true, the transport-layer-averaged horizontal particle velocity \bar{v}_x would be bounded between the horizontal velocities at take-off and impact and thus be approximately proportional to the bed velocity V_b . However, we find that \bar{v}_x scales with the fluid velocity within the transport layer and not with V_b .

Finally, for fully impact-sustained transport, our study predicts a relatively strong negative feedback of the particle motion on the flow for dimensionless fluid shear stress sufficiently close to Θ_t^{ex} . As a consequence, \bar{v}_x , which is controlled by the flow, remains approximately constant with Θ , leading to a linear scaling of the sediment transport rate ($Q \propto \Theta - \Theta_t^{\text{ex}}$). However, for turbulent bedload, this linear scaling becomes non-linear slightly above the threshold ($\Theta \approx 2\Theta_t^{\text{ex}}$) due to a sudden drop in the relative feedback strength, which is associated with the formation of a liquid-like bed of particles on top of the quasi-static bed surface.

Our numerical finding that steady turbulent bedload transport is fully sustained through particle-bed impacts may be criticized because the simulations are quasi-two-dimensional and do only account for the turbulent mean flow, but not for turbulent fluctuations around the mean, which are known to be crucial for the initiation of bedload transport [28–30]. However, we believe that our finding is robust because our simulations quantitatively reproduce measurements of bedload transport cessation thresholds Θ_t^{ex} [12], which would not be expected if these neglected items played a crucial role for entrainment of bed sediment in steady bedload transport. Our reasoning is

supported by Ref. [59], who compared three-dimensional bedload transport simulations with and without turbulent fluctuations. Their Fig. 6 indicates that, although the initiation threshold is strongly affected by turbulent fluctuations, Θ_t^{ex} is nearly unaffected because the extrapolation of the simulated transport rates to vanishing transport remains nearly the same.

We acknowledge support from grants National Natural Science Foundation of China (Nos. 1151101041 and 41376095) and Natural Science Foundation of Zhejiang Province (No. LR16E090001).

* 0012136@zju.edu.cn

- [1] M. Yalin, *Mechanics of Sediment Transport* (Pergamon Press, Oxford, 1977).
- [2] W. H. Graf, *Hydraulics of sediment transport* (Water Resources Publications, Littleton, 1984).
- [3] L. C. van Rijn, *Principles of sediment transport in rivers, estuaries and coastal seas* (Aqua Publications, Amsterdam, 1993).
- [4] P. Y. Julien, *Erosion and Sedimentation* (Cambridge University Press, Cambridge, 1998).
- [5] M. H. Garcia, *Sedimentation engineering: processes, measurements, modeling, and practice* (American Society of Civil Engineers, 2007).
- [6] M. C. Bourke, N. Lancaster, L. K. Fenton, E. J. R. Parteli, J. R. Zimbelman, and J. Radebaugh, *Geomorphology* **121**, 1 (2010).
- [7] R. A. Bagnold, *The physics of blown sand and desert dunes* (Methuen, New York, 1941).
- [8] Y. Shao, *Physics and modelling of wind erosion* (Kluwer Academy, Dordrecht, Amsterdam, 2008).
- [9] O. Durán, P. Claudin, and B. Andreotti, *Aeolian Research* **3**, 243 (2011).
- [10] J. F. Kok, E. J. R. Parteli, T. I. Michaels, and D. B. Karam, *Reports on Progress in Physics* **75**, 106901 (2012).
- [11] A. Valance, K. R. Rasmussen, A. Ould El Moctar, and P. Dupont, *Comptes Rendus Physique* **16**, 105 (2015).
- [12] T. Pähtz and O. Durán, under review in *Nature Astronomy* (2016).
- [13] P. Frey and M. Church, *Science* **325**, 1509 (2009).
- [14] P. Frey and M. Church, *Earth Surface Processes and Landforms* **36**, 58 (2011).
- [15] A. F. Shields, *Application of Similarity Principles and Turbulence Research to Bedload Movement (English translation of the original German manuscript)*, 167 (Hydrodynamics Laboratory, California Institute of Technology, Pasadena, Calif, 1936).
- [16] B. D. Ward, *Water Resources Research* **5**, 1090 (1969).
- [17] L. C. van Rijn, *Journal of Hydraulic Engineering* **110**, 1431 (1984).
- [18] J. M. Buffington and D. R. Montgomery, *Water Resources Research* **33**, 1993 (1997).
- [19] J. M. Buffington, *Journal of Hydraulic Engineering* **125**, 376 (1999).
- [20] S. Dey, *Applied Mathematical Modelling* **23**, 399 (1999).
- [21] S. Dey, *Journal of Hydraulic Research* **41**, 405 (2003).
- [22] D. Paphitis, *Coastal Engineering* **43**, 227 (2001).
- [23] Z. Cao, G. Pender, and J. Meng, *Journal of Hydraulic Engineering* **132**, 1097 (2006).
- [24] S. Vollmer and M. G. Kleinmans, *Water Resources Research* **43**, W05410 (2007).
- [25] A. A. Beheshti and B. Ataie-Ashtiani, *Coastal Engineering* **55**, 423 (2008).
- [26] S. Dey and A. Papanicolaou, *Water Engineering* **12**, 45 (2008).
- [27] A. Recking, *Water Resources Research* **45**, W04401 (2009).
- [28] P. Diplas, C. L. Dancey, A. O. Celik, M. Valyrakis, K. Greer, and T. Akar, *Science* **322**, 717 (2008).
- [29] M. Valyrakis, P. Diplas, C. L. Dancey, K. Greer, and A. O. Celik, *Journal of Geophysical Research* **115**, F02006 (2010).
- [30] M. Valyrakis, P. Diplas, and C. L. Dancey, *Journal of Geophysical Research* **118**, 42 (2013).
- [31] H. Lee, M. Y. Ha, and S. Balachandar, *Physics of Fluids* **24**, 116604 (2012).
- [32] S. Z. Ali and S. Dey, *Physics of Fluids* **28**, 075103 (2016).
- [33] M. Houssais, C. P. Ortiz, D. J. Durian, and D. J. Jerolmack, *Nature Communications* **6**, 6527 (2015).
- [34] G. Maniatis, T. B. Hoey, M. A. Hassan, J. Sventek, R. Hodge, T. Drysdale, M. Valyrakis, and M.ASCE, *Journal of Hydraulic Engineering*, 04016097 (2016).
- [35] L. Roušar, Z. Zachoval, and P. Julien, *Journal of Hydraulic Research* **54**, 615 (2016).
- [36] R. A. Bagnold, *The Geographical Journal* **89**, 409 (1937).
- [37] R. A. Bagnold, *Proceedings of the Royal Society London Series A* **332**, 473 (1973).
- [38] J. E. Ungar and P. K. Haff, *Sedimentology* **34**, 289 (1987).
- [39] R. S. Anderson and P. K. Haff, *Science* **241**, 820 (1988).
- [40] R. S. Anderson and P. K. Haff, *Acta Mechanica Supplementum* **1**, 21 (1991).
- [41] I. K. McEwan and B. B. Willetts, *Acta Mechanica Supplementum* **1**, 53 (1991).
- [42] I. K. McEwan and B. B. Willetts, *Journal of Fluid Mechanics* **252**, 99 (1993).
- [43] J. F. Kok, *Physical Review Letters* **104**, 074502 (2010).
- [44] J. F. Kok, *Geophysical Research Letters* **37**, L12202 (2010).
- [45] T. Pähtz, J. F. Kok, and H. J. Herrmann, *New Journal of Physics* **14**, 043035 (2012).
- [46] J. T. Jenkins and A. Valance, *Journal of Fluid Mechanics* **26**, 073301 (2014).
- [47] D. Berzi, J. T. Jenkins, and A. Valance, *Journal of Fluid Mechanics* **786**, 190 (2016).
- [48] A. H. Clark, M. D. Shattuck, N. T. Ouellette, and C. S. O'Hern, *Physical Review E* **92**, 042202 (2015).
- [49] O. Durán, B. Andreotti, and P. Claudin, *Physics of Fluids* **24**, 103306 (2012).
- [50] M. V. Carneiro, T. Pähtz, and H. J. Herrmann, *Physical Review Letters* **107**, 098001 (2011).
- [51] M. V. Carneiro, N. A. M. Araújo, T. Pähtz, and H. J. Herrmann, *Physical Review Letters* **111**, 058001 (2013).
- [52] O. Durán, B. Andreotti, and P. Claudin, *Advances in Geosciences* **37**, 73 (2014).
- [53] O. Durán, P. Claudin, and B. Andreotti, *Proceedings of the National Academy of Science* **111**, 15665 (2014).
- [54] A. G. Kidanemariam and M. Uhlmann, *Journal of Fluid Mechanics* **750**, R2 (2014).
- [55] A. G. Kidanemariam and M. Uhlmann, *International Journal of Multiphase Flow* **67**, 174 (2014).

- [56] M. W. Schmeckle, *Journal of Geophysical Research: Earth Surface* **119**, 1240 (2014).
- [57] T. Pätz, O. Durán, T.-D. Ho, A. Valance, and J. F. Kok, *Physics of Fluids* **27**, 013303 (2015).
- [58] M. V. Carneiro, K. R. Rasmussen, and H. J. Herrmann, *Scientific Reports* **5**, 1 (2015).
- [59] R. Maurin, J. Chauchat, B. Chareyre, and P. Frey, *Physics of Fluids* **27**, 113302 (2015).
- [60] R. Maurin, J. Chauchat, and P. Frey, *Journal of Fluid Mechanics* **804**, 490 (2016).
- [61] B. Andreotti, *Journal of Fluid Mechanics* **510**, 47 (2004).
- [62] L. Oger, M. Ammi, A. Valance, and D. Beladjine, *European Physical Journal E* **17**, 467 (2005).
- [63] P. Claudin and B. Andreotti, *Earth and Planetary Science Letters* **252**, 30 (2006).
- [64] D. Beladjine, M. Ammi, L. Oger, and A. Valance, *Physical Review E* **75**, 061305 (2007).
- [65] L. Oger, M. Ammi, A. Valance, and D. Beladjine, *Computers and Mathematics with Applications* **55**, 132 (2008).
- [66] X. Y. Zou, Z. L. Wang, Q. Z. Hao, C. L. Zhang, Y. Z. Liu, and G. R. Dong, *Geomorphology* **36**, 155 (2001).
- [67] S. L. Namikas, *Sedimentology* **50**, 303 (2003).
- [68] Z. Dong, X. Liu, X. Wang, F. Li, and A. Zhao, *Earth Surface Processes and Landforms* **29**, 343 (2004).
- [69] K. R. Rasmussen and M. Sørensen, *Journal of Geophysical Research* **113**, F02S12 (2008).
- [70] M. Creyssels, P. Dupont, A. Ould El Moctar, A. Valance, I. Cantat, J. T. Jenkins, J. M. Pasini, and K. R. Rasmussen, *Journal of Fluid Mechanics* **625**, 47 (2009).
- [71] T. D. Ho, A. Valance, P. Dupont, and A. Ould El Moctar, *Physical Review Letters* **106**, 094501 (2011).
- [72] J. A. Simeonov and J. Calantoni, *International Journal of Multiphase Flow* **46**, 38 (2012).
- [73] P. Gondret, M. Lance, and L. Petit, *Physics of Fluids* **14**, 2803 (2002).
- [74] F. L. Yang and M. L. Hunt, *Physics of Fluids* **18**, 121506 (2006).
- [75] See supplementary materials for technical details, additional information, and movie captions.
- [76] M. Ouriemi, P. Aussillous, M. Medale, Y. Peysson, and E. Guazzelli, *Physics of Fluids* **19**, 061706 (2007).
- [77] M. Lämmel, D. Rings, and K. Kroy, *New Journal of Physics* **14**, 093037 (2012).
- [78] G. M. Smart, *Journal of Hydraulic Engineering* **110**, 267 (1984).
- [79] E. Lajeunesse, L. Malverti, and F. Charru, *Journal of Geophysical Research* **115**, F04001 (2010).
- [80] H. Capart and L. Fraccarollo, *Geophysical Research Letters* **38**, L20402 (2011).
- [81] R. A. Bagnold, *Proceedings of the Royal Society London Series A* **157**, 594 (1936).
- [82] R. A. Bagnold, *Proceedings of the Royal Society London Series A* **167**, 282 (1938).
- [83] K. R. Rasmussen, J. D. Iversen, and P. Rautahemio, *Geomorphology* **17**, 19 (1996).
- [84] R. L. Martin and J. F. Kok, (2016), <https://arxiv.org/abs/1609.09458v1>.
- [85] D. M. Burr, N. T. Bridges, J. R. Marshall, J. K. Smith, B. R. White, and J. P. Emery, *Nature* **517**, 60 (2015).
- [86] R. Kawamura, in *Translated (1965) as University of California Hydraulics Engineering Laboratory Report HEL 2 Berkeley* (1951).
- [87] P. R. Owen, *Journal of Fluid Mechanics* **20**, 225 (1964).
- [88] R. J. Kind, *Atmospheric Environment* **10**, 219 (1976).
- [89] K. Lettau and H. H. Lettau, in *IES Report*, Vol. 101 (1978) pp. 110–147.
- [90] M. Sørensen, *Acta Mechanica Supplementum* **1**, 67 (1991).
- [91] M. Sørensen, *Geomorphology* **59**, 53 (2004).
- [92] G. Sauermann, K. Kroy, and H. J. Herrmann, *Physical Review E* **64**, 31305 (2001).
- [93] O. Durán and H. J. Herrmann, *Journal of Statistical Mechanics* **2006**, P07011 (2006).

TECHNICAL COMPUTATION DETAILS

Local, mass-weighted ensemble average

We compute the local, mass-weighted ensemble average $\langle A \rangle$ of a particle quantity A through [57]

$$\langle A \rangle = \frac{1}{\rho} \overline{\sum_n m^n A^n \delta(\mathbf{x} - \mathbf{x}^n)}^E, \quad (\text{S1})$$

$$\rho = \overline{\sum_n m^n \delta(\mathbf{x} - \mathbf{x}^n)}^E, \quad (\text{S2})$$

where m is particle mass, \mathbf{x} the location, and δ the delta distribution. Furthermore, the sum iterates over all particles ($n \in (1, N)$), with N the total number of particles), and $\overline{\cdot}^E$ denotes the ensemble average.

Particle stress tensor

Using the definition of the local, mass-weighted ensemble average, we obtain the particle stress tensor P_{ij} through [57]

$$P_{ij} = \rho \langle v'_i v'_j \rangle + \frac{1}{2} \overline{\sum_{mn} F_j^{mn} (x_i^m - x_i^n) K(\mathbf{x}, \mathbf{x}^m, \mathbf{x}^n)}^E, \quad (\text{S3})$$

$$\mathbf{v}' = \mathbf{v} - \langle \mathbf{v} \rangle, \quad (\text{S4})$$

$$K = \int_0^1 \delta(\mathbf{x} - ((\mathbf{x}^m - \mathbf{x}^n)s + \mathbf{x}^n)) ds, \quad (\text{S5})$$

where \mathbf{v} is the particle velocity and \mathbf{F}^{mn} the contact force applied by particle n on particle m ($\mathbf{F}^{mm} = 0$).

Rebound height and bed friction coefficient

The bed friction coefficient μ_b is the friction coefficient $\mu = -P_{zx}/P_{zz}$ evaluated at the ‘bed surface’, which is, ideally, the vertical location at which particle-bed impacts occur. However, in a real system, particle-bed impacts are not localized at a fixed vertical location, but their range of influence rather involves several vertical layers of particles. We are thus looking for a definition

of μ_b that involves several particle layers around the bed surface. One way to do so is to exploit the fact that the average horizontal particle velocity $\langle v_x \rangle$ decays exponentially within the sediment bed [33, 49], which implies that $d\langle v_x \rangle/dz$ exhibits a pronounced local maximum near the bed surface. This behavior suggests an approximate definition of μ_b as

$$\mu_b \approx \frac{\max\left(-P_{zx} \frac{d\langle v_x \rangle}{dz}\right)}{\max\left(P_{zz} \frac{d\langle v_x \rangle}{dz}\right)}. \quad (\text{S6})$$

Since the local maxima of $-P_{zx}d\langle v_x \rangle/dz$ and $P_{zz}d\langle v_x \rangle/dz$ in our simulations occur at almost the same location, we define μ_b in the paper as

$$\mu_b = \mu(z_r), \quad (\text{S7})$$

where the location z_r is defined through

$$\max\left(P_{zz} \frac{d\langle v_x \rangle}{dz}\right) = \left[P_{zz} \frac{d\langle v_x \rangle}{dz}\right](z_r) \quad (\text{S8})$$

The term $-P_{zx}d\langle v_x \rangle/dz = \mu_b P_{zz}d\langle v_x \rangle/dz$ is the particle shear work, due to which fluctuation energy is produced [57]. Since, in a steady system, the location of maximal fluctuation energy production approximately corresponds to the location of maximal fluctuation energy dissipation, z_r should approximately correspond to the location where energetic rebounds of transported particles occur, which is usually near the bed surface. However, when sediment transport is sufficiently intense, a liquid-like bed can develop, and the most energetic rebounds occur near the liquid-bed surface rather than the quasi-static bed surface [51].

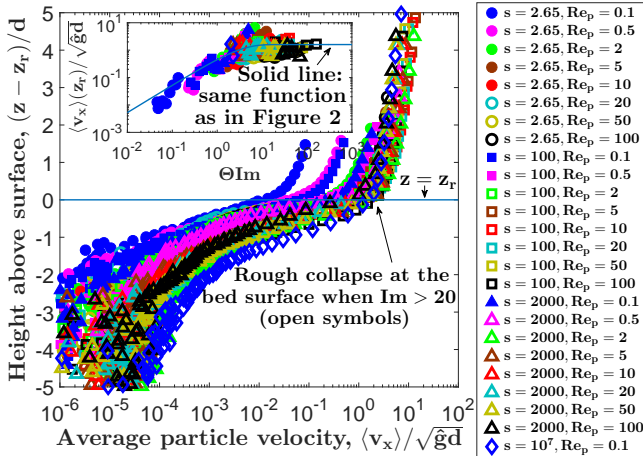


FIG. S1. Vertical profiles of $\langle v_x \rangle/\sqrt{gd}$ for various s and Re_p near threshold conditions ($\Theta \cong \Theta_t^{\text{ex}}$). Inset: $\langle v_x \rangle(z_r)/\sqrt{gd}$ versus ΘIm .

Bed velocity

Like for μ_b , we are looking for a definition of the bed velocity V_b that involves several particle layers around the bed surface because particle-bed impacts are not localized at a fixed vertical location. The fact that z_r is an approximation of the effective location of the bed surface for non-intense sediment transport suggests that an appropriate definition of V_b should have the property that it can be approximated through $V_b \approx \langle v_x \rangle(z_r)$ (i.e., the classical definition of the slip velocity [70]) sufficiently near the threshold (Θ_t^{ex}). Indeed, Fig. S1 and its inset show that the vertical profiles of $\langle v_x \rangle/\sqrt{gd}$ for fully impact-sustained conditions near Θ_t^{ex} tend to approach a roughly constant value ($\langle v_x \rangle(z_r)/\sqrt{gd} \approx 0.5-1.5$), and that $\langle v_x \rangle(z_r)/\sqrt{gd}$ as a function of ΘIm roughly follows the same behavior as V_b/\sqrt{gd} in Fig. 2. Fig. S1 also shows that the exponential decay of $\langle v_x \rangle$ within the sediment bed occurs within a characteristic decay height proportional to d . This implies

$$V_b \propto V'_b d, \quad (\text{S9})$$

where V'_b is a characteristic horizontal velocity gradient near the bed surface. We calculate V'_b as the ratio between $\max(-P_{zx}d\langle v_x \rangle/dz)$, which is a suitable definition of an effective bed surface value of $-P_{zx}d\langle v_x \rangle/dz$ (see Eqs. (S8)), and a suitable definition of the bed-surface-averaged particle shear stress $-P_{zx}$, namely,

$$V'_b = \frac{\max\left(-P_{zx} \frac{d\langle v_x \rangle}{dz}\right)}{\frac{1}{\rho_b} \int_{-\infty}^{\infty} \frac{d\rho}{dz} P_{zx} dz}, \quad (\text{S10})$$

where the weight $-\rho_b^{-1}d\rho/dz$, with $\rho_b \approx 0.58\rho_p$ the value of the particle concentration ρ deep within the bed, is maximal near the bed surface because it vanishes sufficiently within and above the bed. After partial integration, using $-P_{zx}(-\infty) = \tau$ and the horizontal momentum balance $dP_{zx}/dz = \rho\langle a_x \rangle$ [57], with \mathbf{a} the particle acceleration due to non-contact forces, Eq. (S10) becomes

$$V'_b = \frac{\max\left(-P_{zx} \frac{d\langle v_x \rangle}{dz}\right)}{\tau - \frac{1}{\rho_b} \int_{-\infty}^{\infty} \rho^2 \langle a_x \rangle dz}. \quad (\text{S11})$$

Finally, we obtain the proportionality factor in Eq. (S9) by imposing that the bed velocity approximately equals the classical slip velocity, $V_b \approx \langle v_x \rangle(z_r)$, for the simulated turbulent saltation cases ($s = 2000$, $Re_p \geq 5$) in order to be consistent with the classical definition for turbulent saltation transport [70]. This constraint yields

$$V_b = 0.5d \times \frac{\max\left(-P_{zx} \frac{d\langle v_x \rangle}{dz}\right)}{\tau - \frac{1}{\rho_b} \int_{-\infty}^{\infty} \rho^2 \langle a_x \rangle dz}. \quad (\text{S12})$$

Relative rebound height

We define the location z_s of the interface between transport layer and quasi-static bed as the location at which the friction coefficient is equal to $0.7\mu_b$, reading

$$\mu(z_s) = 0.7\mu_b, \quad (\text{S13})$$

This definition accounts for potential dependencies of the interface location z_s on the contact friction coefficient μ^c . For a typical value $\mu_b = 0.6$, it corresponds to $\mu(z_s) = 0.42$, consistent with previous studies of bedload transport [59]. We use Eq. (S13) to define the relative rebound height as

$$\Delta z_r = z_r - z_s. \quad (\text{S14})$$

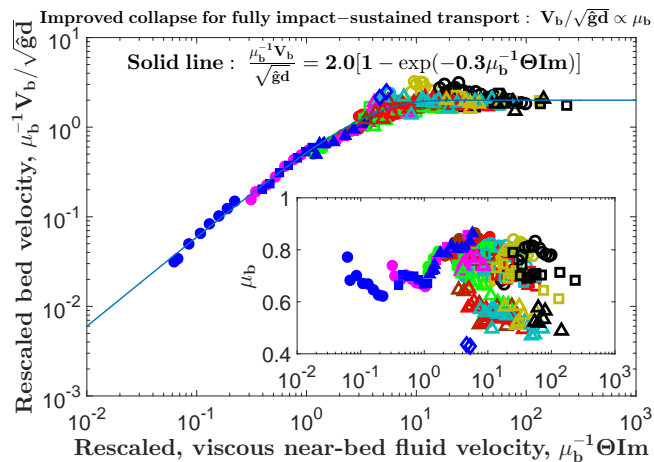


FIG. S2. Dimensionless bed velocity V_b/\sqrt{gd} , computed by Eq. (S12), versus dimensionless, viscous, horizontal near-bed fluid velocity ΘIm , both rescaled by μ_b , for various s , Re_p , and Θ . Inset: Bed friction coefficient μ_b versus $\mu_b^{-1} \Theta St$. For symbol legend, see Fig. S1.

Role of bed friction in fully impact-sustained transport

Fig. S2 shows that the data collapse in Fig. 2 of the paper is much improved when rescaling both axes by μ_b . This is because larger bed friction makes it more difficult to entrain particles through impacts, leading to an increased bed velocity that is required for fully impact-sustained transport ($V_b/\sqrt{gd} \propto \mu_b$).

Transport layer average

We compute the transport layer average \bar{A} of a particle quantity A via [12]

$$\bar{A} = \frac{\int_{z_r}^{\infty} \rho \langle A \rangle dz}{\int_{z_r}^{\infty} \rho dz}. \quad (\text{S15})$$

It describes a mass-weighted average of A over all particles within the transport layer defined through $z > z_r$.

MOVIE CAPTIONS

Movie S1

Time evolution of the simulated particle-fluid system for $s = 2000$, $\text{Re}_p = 20$, and $\sqrt{\Theta} = 0.08$, considering weakly-damped binary collisions ($e = 0.9$). The flow velocity is shown as a background color with warm colors corresponding to high velocities and cold colors to small velocities. The horizontal and vertical axes are measured in mean particle diameters. Only 1/4 of the simulated horizontal domain is shown, which is why there are occasions at which no moving particle can be observed. This is an example for saltation transport, which is predominantly sustained through particle-bed impact entrainment. One can see that impacting particles tend to eject surface particles.

Movie S2

Time evolution of the simulated particle-fluid system for $s = 2.65$, $\text{Re}_p = 20$, and $\sqrt{\Theta} = 0.33$, considering binary collisions that are nearly fully damped by the lubrication force ($e = 0.01$). The flow velocity is shown as a background color with warm colors corresponding to high velocities and cold colors to small velocities. The horizontal and vertical axes are measured in mean particle diameters. Only 1/4 of the simulated horizontal domain is shown, which is why there are occasions at which no moving particle can be observed. This is an example for turbulent bedload transport, which is predominantly sustained through particle-bed impact entrainment. One can see that impacting particles tend to drag surface particles out of they traps.

Movie S3

Time evolution of the simulated particle-fluid system for $s = 2000$, $\text{Re}_p = 20$, and $\sqrt{\Theta} = 0.17$, considering weakly-damped binary collisions ($e = 0.9$). The flow velocity is shown as a background color with warm colors corresponding to high velocities and cold colors to small

velocities. The horizontal and vertical axes are measured in mean particle diameters. Only 1/4 of the simulated horizontal domain is shown, which is why there are occasions at which no moving particle can be observed. This is an example for saltation transport, which is predominantly sustained through particle-bed impact entrainment. One can see that impacting particles tend to eject surface particles.

Movie S4

Time evolution of the simulated particle-fluid system for $s = 2.65$, $\text{Re}_p = 20$, and $\sqrt{\Theta} = 0.66$, considering

binary collisions that are nearly fully damped by the lubrication force ($e = 0.01$). The flow velocity is shown as a background color with warm colors corresponding to high velocities and cold colors to small velocities. The horizontal and vertical axes are measured in mean particle diameters. Only 1/4 of the simulated horizontal domain is shown. This is an example for turbulent bedload transport, which is predominantly sustained through particle-bed impact entrainment. However, it is impossible to determine single entrainment events as several layers of the bed are in continuous motion. These layers constitute the liquid-like bed, and it can be seen that energetic particles tend to rebound from its top.

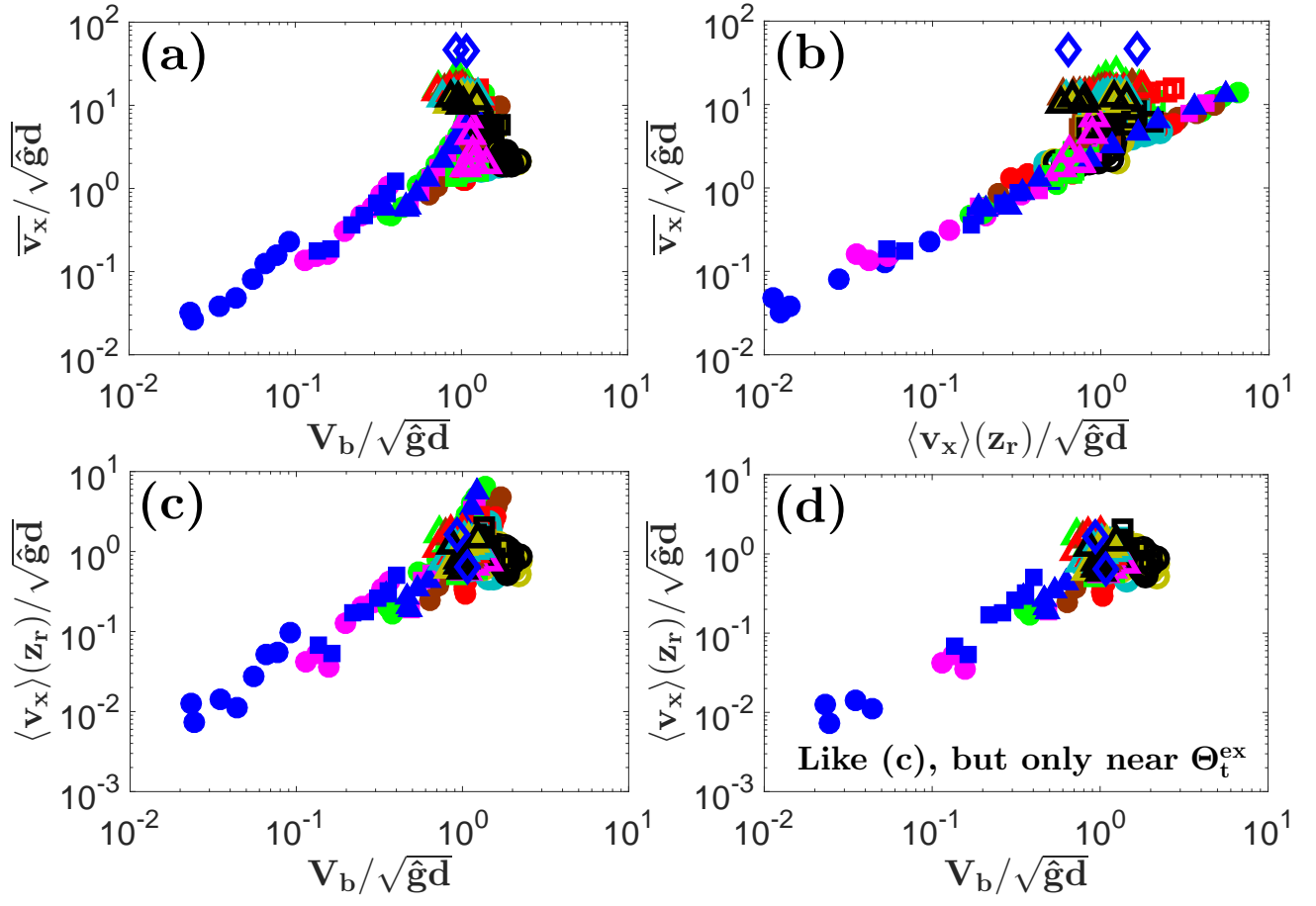


FIG. S3. Correlation between average horizontal particle velocity $\overline{v_x}$ and (a) bed velocity V_b and (b) classical slip velocity $\langle v_x \rangle(z_r)$. It can be seen that they only correlate for non-fully impact-sustained sediment transport. (c) Correlation between $\langle v_x \rangle(z_r)$ and V_b . (d) Same as (c), but only conditions close to the threshold. It can be seen that, near the threshold, $\langle v_x \rangle(z_r)$ and V_b are roughly of similar magnitude. For symbol legend, see Fig. S1.